Fluid–fluid coexistence in colloidal systems with short-ranged strongly directional attraction

Norbert Kern[a] and Daan Frenkel[b]
FOM Institute for Atomic and Molecular Physics, Kruislaan 407, 1098 SJ Amsterdam, The Netherlands

(Received 17 June 2002; accepted 3 March 2003)

We present a systematic numerical study of the phase behavior of square-well fluids with a ''patchy'' short-ranged attraction. In particular, we study the effect of the size and number of attractive patches on the fluid–fluid coexistence. The model that we use is a generalization of the hard sphere square well model. The systems that we study have a stronger tendency to form gels than the isotropic square-well system. For this reason, we had to combine Gibbs ensemble simulations of the fluid–fluid coexistence with a parallel tempering scheme. For moderate directionality, changes of the critical density and the width of coexistence curves are small. For strong directionality, however, we find clear deviations from the extended law of corresponding states: in contrast to isotropic attractions, the critical point is *not* characterized by a universal value of the reduced second virial coefficient. Furthermore, as the directionality increases, multiparticle bonding affects the critical temperature. We discuss implications for the phase behavior, and possibly crystallization, of globular proteins. © *2003 American Institute of Physics.* [DOI: 10.1063/1.1569473]

I. INTRODUCTION

Many fluids, both simple and complex, exhibit coexistence of a liquid and a vapor phase in some part of their phase diagram. In the simplest case, this feature can be reproduced by the van der Waals equation of state, where particle interactions are described by their excluded volume and a mean-field attractive energy only.[1] Liquid–vapor-like transitions occur not only for simple atoms and molecules, but also in suspensions of colloids and (bio) macromolecules such as proteins (see, e.g., Ref. 2). In protein solutions, each particle consists of thousands of atoms. As a result, the pair interaction between two protein molecules is much more complex than that between atoms or spherical colloids. It is clearly desirable to know how the interaction between proteins in solution affects their phase behavior. Unfortunately, while it is in principle possible to compute the effective interaction between two protein molecules in solution, such calculations are extremely time consuming and are, at present, barely feasible. Experiments yield only partial information on the interaction between proteins: either through their osmotic compressibility at low concentrations, or through the structure of the crystals that they form. In practice, there is no unique way to deduce a pair potential from this information. Hence there is, at present, no direct way to predict the phase behavior of protein solutions. Still, measurements of the collective behavior of protein solutions make it possible to obtain at least some average information on the protein–protein interactions. This approach has been employed by George and Wilson,[3] who showed that, under crystallization conditions, the value of the (reduced) second osmotic virial coefficient of globular proteins falls within a rather narrow range. This observation was generalized by Rosenbaum *et al.*,[4] who demonstrated that a model of hard spheres with an isotropic short-ranged attraction is a useful starting point for describing the phase behavior of many solutions of globular proteins.

The fact that, to a first approximation, globular proteins can be described as hard spheres with short-ranged attraction, makes it possible to exploit parallels with colloidal systems that can be described with a similar model. One particularly striking feature of the phase diagram of hard spheres with short-ranged attraction is the disappearance of a stable fluid–fluid coexistence curve. A transition between two stable fluid phases of different densities is only possible for relatively long-ranged attractions. For shorter ranges (shorter than a value between roughly 10% and 30% of the particle diameter, depending on the particular model used) the fluid–fluid coexistence becomes *metastable*.[5,6] Although not an equilibrium phase, the presence of a fluid–fluid critical point can substantially lower the free energy barrier for nucleation of a crystalline germ, and can thus indirectly promote the crystallization.[7] Understanding fluid–fluid phase coexistence is thus an integral part of studying the phase behavior of protein solutions, as it may be an important ingredient toward predicting suitable crystallization conditions. Among the results that have emerged in the context of simple fluid models is the remarkable fact that the reduced second virial coefficient (i.e., the value of B_2 relative to its equivalent for the corresponding hard-sphere model) has an approximately constant value at the critical temperature for fluid–fluid coexistence.[8] This value appears to depend only weakly on the precise form of the interparticle potential.[8,9] This makes it possible to focus on simple models (e.g., hard spheres with an attractive square well, HSSW), since systems with complicated potentials can be mapped onto such simpler model systems.[9]

There is, however, an important limitation in the work of

[a]Present address: Physics Department, Trinity College, Dublin, Ireland.
[b]Electronic mail: frenkel@amolf.nl

 © 2003 American Institute of Physics

Downloaded 11 Oct 2004 to 145.18.129.130. Redistribution subject to AIP license or copyright, see http://jcp.aip.org/jcp/copyright.jsp

Refs. 8 and 9: both papers only consider potentials that are independent of the relative orientation of the interacting molecules. This simplifying assumption is certainly not justified in the case of protein interactions. It is therefore important to identify the differences between the phase behavior of simple isotropic model systems and that of the more general models with anisotropic interactions. Anisotropy in protein–protein interactions may be due to various physical mechanisms: interactions between nonuniformly distributed surface charges, the presence of hydrophyllic/hydrophobic zones on the protein surface, and the formation of hydrogen bonds at specific surface locations. Several groups[10–13] have provided evidence that isotropic interaction models cannot properly account for experimentally observed phase diagrams of protein solutions.

Theoretical models have been put forward in order to take into account the effect of directionality of short-ranged attractive forces on the fluid–solid phase boundaries.[11,14] The Sear model,[14] and variations of it, have also been used to interpret experimental data on fluid–fluid coexistence in protein solutions.[12,13] Models of this class are formulated in terms of ''binding sites,'' represented by off-center attractive square well potentials, localized at the particle surface, and they can be treated in the framework of the Wertheim theory of associating fluids.[15–17] This perturbative approach allows one to deduce an analytical equation of state for the fluid. However, the theory does not take into account formation of ring-like clusters (at least not in a first-order formulation). Moreover, it assumes that the structure of the associating fluid can be modeled by that of a hard-sphere fluid. The theory is thus intrinsically limited to the ''weak bonding'' regime, and it may be less suited to obtain accurate data on the fluid–fluid coexistence in the case of highly directional interactions.[13] Numerical work on these systems has been presented by Vega and Monson,[18] who determine coexistence curves involving solid phases for a particular set of parameters and particles with tetrahedral symmetry, aimed at mimicking the phase behavior of water. Fluid–fluid coexistence, however, has not been studied numerically.

An alternative class of models has been proposed by Lomakin *et al.*[10] In this work, the attraction is localized on patches of the protein surface. For one particular representative of these models, the authors have used numerical arguments to deduce an equation of state, thus enabling them to compare phase diagrams to experimental data on proteins.[10] The approach of Ref. [10] relies on the hypothesis that an effective interparticle potential (strictly speaking, a free energy) can be obtained by orientational preaveraging of the Boltzmann factor associated with the pair interactions.

In the present paper, we wish to approach the problem of the phase behavior of systems with directional attractions by direct computer simulation. To do so, we formulate a simple generic model for directional attraction in terms of a pair potential, designed to separate effects of range and anisotropy of the attractions. Next, we present Monte Carlo simulations that explore how the directionality affects the fluid–fluid coexistence.

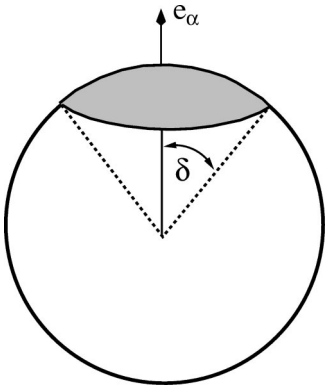

FIG. 1. Illustration of patch definition. A patch α is described by a solid angle (half opening angle δ about an axis $\hat{e}_\alpha$). Two particles attract if their separation vector $\mathbf{r}_{ij}$ intersects some patch (not necessarily the same one) on both particles, *and* if they are within range.

II. MODEL

Our aim is to study a model for particles with strongly directional interactions. Rather than elaborating models for specific protein molecules, we choose to focus on a simple model that can represent a strong directionality of attractions. To this end, we consider ''patchy'' attractive HSSW particles. Two particles attract if they are within a predefined range and the vector joining their center of mass intersects an attractive patch on the surface of *both* particles. Such patchy spheres can be considered as a schematic model for the interaction between protein surfaces where strong short-ranged attractions can exist between hydrophobic regions of the surfaces on different proteins. We define the pair potential as a product of a square-well potential with an angular modulation

$$u_{ij}(r_{ij};\tilde{\Omega}_i,\tilde{\Omega}_j)=u_{ij}^{\mathrm{hssw}}(r_{ij})\cdot f(\tilde{\Omega}_i,\tilde{\Omega}_j), \tag{1}$$

where the radial dependence is given by the regular square-well potential of reduced range λ,

$$u_{ij}^{\mathrm{hssw}}(r)=\begin{cases}\infty & \text{for} \quad r<\sigma \\ -\epsilon & \text{for} \quad \sigma\leqslant r<\lambda\sigma \\ 0 & \text{for} \quad \lambda\sigma\leqslant r.\end{cases} \tag{2}$$

For the orientational dependence, we associate attractive interactions with patches $\alpha=1,\ldots,n$ on the surface of the particles, each corresponding to a conical segment of (half) opening angle δ around the direction $\hat{e}_\alpha$ (cf. Fig. 1). In our model we did not allow patches to overlap, although this restriction is not essential. All particles carry identical patches in a body-fixed frame of reference, but the patch orientations $\hat{e}_\alpha$ are modified as the particles rotate. The angular modulation of the interaction is taken to depend on the direction $\hat{r}_{ij}$ of the particle separation vector $\mathbf{r}_{ij}$, but also on the particle orientations $\tilde{\Omega}_i$, $\tilde{\Omega}_j$, as

Downloaded 11 Oct 2004 to 145.18.129.130. Redistribution subject to AIP license or copyright, see http://jcp.aip.org/jcp/copyright.jsp

$$f_{ij}(\hat{r}_{ij};\tilde{\Omega}_i,\tilde{\Omega}_j)=\begin{cases}1 & \text{if } \begin{cases} & (\hat{e}_\alpha\cdot\hat{r}_{ij}\leqslant\cos\ \delta) \quad \text{for some patch } \alpha \text{ on } i \\ \text{and} & (\hat{e}_\beta\cdot\hat{r}_{ji}\leqslant\cos\ \delta) \quad \text{for some patch } \beta \text{ on } j \end{cases} \\ 0 & \text{otherwise}\end{cases} . \tag{3}$$

Attraction is thus limited to configurations where two patches face each other. Similar models have been used, e.g., by Ghonasgi and Chapman[19] as a perturbation potential to a Lennard-Jones interaction, tailored to modeling water (tetrahedral arrangement of patches with particular binding energies for the individual sites).

Properties of the model potential. The proposed model strictly separates radial and angular features, thus allowing us to assess the effect of both separately. The choice of a discontinuous radial potential is convenient as it makes it possible to give an unambiguous definition to the particle size (here given by the hard core diameter σ). The model potential defines the radial dependence in terms of particle properties (patches). The case considered here is the simplest one (all patches attractive, with identical binding energies and patch sizes), but generalizations to more complex models are straightforward.

In the following, we will be interested in the effect of the reduced attraction range λ, the number n of attractive patches, and their size (described by the angle δ). Note that the intermolecular interactions can be made less isotropic either by decreasing the number of patches or by decreasing the size of individual patches. To facilitate the comparison between different geometries, it is convenient to characterize the size of the patches in terms of the total *surface coverage* χ (percentage of the particle surface covered by patches). χ is related to the number of patches and their size by

$$\chi=n\cdot\sin^2\left(\frac{\delta}{2}\right). \tag{4}$$

The simplicity of the model allows us to write down an analytic expression for the second virial coefficient B_2, which characterizes the effective interaction between particles:

$$B_2=-\frac{1}{2V}\int d^3r_1\int d\tilde{\Omega}_1\int d^3r_2\int d\tilde{\Omega}_2[e^{-\beta u(1,2)}-1], \tag{5}$$

where $\beta=1/k_BT$ as usual, with the Boltzmann constant k_B. The angular integrations, represented by the solid angles $d\tilde{\Omega}$, stand for integration over all particle orientations. For the patchy HSSW model, the integrals can be evaluated analytically, yielding

$$\frac{B_2}{B_2^{\mathrm{HS}}}=1-\chi^2\cdot(\lambda^3-1)\cdot(e^{+\epsilon/kT}-1), \tag{6}$$

where $B_2^{\mathrm{HS}}=2\pi\sigma^3/3$ stands for the virial coefficient associated with hard spheres of diameter σ.

In order to facilitate comparison with the literature on isotropic potentials, we use the expression for B_2 to define the "stickiness" coefficient $1/\tau$, introduced by Baxter in the context of the adhesive-sphere model:[20]

$$\frac{B_2}{B_2^{\mathrm{HS}}}\equiv 1-\frac{1}{4\tau}. \tag{7}$$

For the present model, $1/\tau$ is thus given by

$$\frac{1}{\tau}=4\cdot\chi^2\cdot(\lambda^3-1)\cdot(e^{+\epsilon/kT}-1). \tag{8}$$

The coefficient τ can be considered to be a measure of the temperature. As Eq. (8) shows, τ is a monotonically increasing (but nonlinear) function of T. For a given set of parameters (λ,ϵ,χ) Eqs. (7) and (8) allow us to relate the critical temperature to a corresponding "critical" virial coefficient.

III. SIMULATION TECHNIQUES

The *isotropic* HSSW system has been studied numerically by a large number of authors. While the earlier numerical work often focused on square-well widths that were considered to be typical for simple liquids, more recent studies have explored the wider range of widths of the attractive wells.[21–23] Work by Vega *et al.*,[24] based on Gibbs ensemble simulations, has provided accurate reference data on the critical behavior of isotropic HSSW systems for ranges down to $\lambda=1.25$. We have generalized both Gibbs ensemble and *NVT* simulation techniques to perform simulations on nonisotropic particle interactions.

A. Gibbs ensemble

In order to establish the fluid–fluid coexistence curves (binodals) for systems consisting of "patchy" HSSW particles, we used Gibbs ensemble simulations.[25–28] We performed such simulations for varying surface coverage χ, patch number n, and interaction range λ. Whilst it is straightforward to establish fluid–fluid coexistence for isotropic particles with moderate ranges ($\lambda\geqslant 1.5$), equilibration becomes more difficult for shorter ranges and for strongly directional attractions. For low temperatures (below $k_BT/\epsilon\simeq 0.5$, the precise value depending on the range and the patchiness of the potential) the simulations become prohibitively expensive. This imposes a significant restriction on the temperature range that can be studied, which indeed prevents access to the coexistence region for strongly anisotropic potentials. In order to obtain coexistence curves for strongly directional potentials, and particularly so for shorter ranges, it was necessary to make use of more sophisticated simulations schemes that we briefly describe in the following.

Using the Gibbs ensemble method, we have performed simulations with two different ranges of attraction ($\lambda=1.50$

Downloaded 11 Oct 2004 to 145.18.129.130. Redistribution subject to AIP license or copyright, see http://jcp.aip.org/jcp/copyright.jsp

and $\lambda = 1.25$, respectively). All simulations were carried out with $N = 512$ particles. The overall density used for the longer range was $\rho_{tot} = 0.30$, and $\rho_{tot} = 0.40$ for the shorter range. Within each simulation cycle we attempted $N = 512$ particle displacements and the same number of particle rotations. Furthermore, two attempts at exchanging volume were made per cycle. The number of attempted particle exchanges per cycle was variable, adjusted during equilibration runs as to target an exchange of about 2% (on average) of all particles during a cycle; this typically required 500 attempts for the longer range, and up to a few thousand attempts for the shorter range. Equilibration was for a minimum of 500 000 cycles for the longer range, with production runs of at least another 500 000 cycles. For the shorter range, equilibration and production lasted a minimum of one million cycles each (some substantially longer).

To estimate the critical temperature and the critical density for each set of parameters, we assumed that the densities of the coexisting phases and of the critical point were related through the law of rectilinear diameter:[29]

$$(\rho_{liq} + \rho_{gas})/2 = \rho_c + A \cdot |T - T_c|, \tag{9}$$

$$\rho_{liq} - \rho_{gas} = B \cdot |T - T_c|^{0.32}. \tag{10}$$

This fit also supplies an estimate for the width of the coexistence curves, $b = B \cdot Tc^{0.32}$, which characterizes the width of the binodals in terms of the dimensionless temperature relative to the critical point, $t = |T/T_c - 1|$.

B. Parallel tempering (*NVT*)

The parallel tempering method is often used to simulate systems that have a very rugged potential energy landscape.[30,28] In a parallel tempering simulation, several Monte Carlo runs, each at a different temperature, are performed in parallel. To speed up equilibration, special swapping moves are introduced that exchange configurations belonging to different temperatures. The underlying idea is that coupling to high temperatures leads to more efficient sampling of configuration space. Systems that, at low temperatures, would be stuck in the environment of one particular local energy minimum, can escape to other local minima by ''diffusing'' up (and subsequently down) in temperature. The acceptance probability for a swap of system i, initially at temperature T_i, and system j, initially at temperature T_j, is

$$P = \min\left(1, \exp - \left(\frac{1}{T_i} - \frac{1}{T_j}\right) \cdot (E_j - E_i)\right). \tag{11}$$

This condition[30,28] guarantees that all the individual subsystems are maintained in thermal equilibrium. The communication overhead between configurations, required for the swapping moves, is small, and we have therefore implemented the simulations in a parallel fashion.

In order to achieve a reasonable acceptance probability of such parallel-tempering moves, the temperature difference between systems i and j should not be too large. Moreover, the configurations in the two systems should be energetically similar. The parallel-tempering scheme can be used in various ensembles. We found it most convenient to work with systems at fixed volume. This obviates the need to select a ''reasonable'' initial pressure, which would be difficult. In addition, we avoid the problem that, inside the binodal, large density changes may occur in systems at constant pressure. We have simulated $N_{sys} = 24$ subsystems, each at a different temperature, attempting a configuration swap between neighboring levels after a fixed number of sweeps for *each* level. In order to be able to explore a large range of the various parameters, we had to ensure that individual simulations were cheap. We therefore used rather small systems with $N = 128$ particles. For the present study, this is not a serious restriction, since our main goal is to identify trends, and the available literature data on the isotropic HSSW system suggest that even these rather small system sizes allow a fair estimate of the critical temperature. Temperature differences between neighboring levels were chosen sufficiently small to ensure good acceptance of swapping moves.

For each set of parameters for the interaction potential (range, surface coverage, patch number and geometry), this method requires simulating a series of such runs, at several densities, yielding $N_{sys} = 24$ pressure–temperature pairs each; this effectively establishes $N_{sys} = 24$ isotherms. It is typically easy to identify those isotherms corresponding to temperatures just above and just below the critical temperature, and since the spacing of temperature levels is very narrow in this region, this gives a very straightforward estimate for the critical temperature T_c. The critical density on the other hand cannot be determined in this way with any degree of accuracy; this would require fitting the data to a model for the equation of states. We have not attempted to do so here.

C. Pressure calculations

An additional technical complication arises in pressure measurements: the usual way of evaluating the virial contribution through interparticle forces[28] cannot easily be applied due to the discontinuities in the radial potential. However, the discontinuities in the interaction energy are reflected in the radial distribution function $g(r)$, and the pressure can be obtained from the latter through an extrapolation procedure.[31,32,1] The underlying relation is the link between the compressibility factor and the radial distribution function $g(r)$ (see, e.g., Hansen and MacDonald[1]):

$$\frac{\beta P}{\rho} = 1 - \frac{2\pi}{3} \cdot \beta\rho \int_0^\infty r_{12}^3 \left\langle g(1,2) \cdot \frac{du}{dr_{12}} \right\rangle dr_{12}, \tag{12}$$

where $\langle . \rangle$ denotes an angular (i.e., nonweighted) average. Smith *et al.*[31] showed how the integrals are to be evaluated for piecewise constant potentials in the case of isotropic interactions. This method has been used by various authors in the context of isotropic HSSW potentials (e.g., Refs. 23 and 22). For the ''patchy'' potential [Eqs. (1)–(3)] this approach can be shown to generalize to

$$\frac{\beta P}{\rho} = 1 + \frac{2\pi}{3} \rho\sigma^3 [g(\sigma^+) - \lambda^3 \cdot (g_{pp}(\lambda\sigma^-) - g_{pp}(\lambda\sigma^+))] \tag{13}$$

where $g_{pp}(r)$ is the radial patch–patch distribution function, i.e., the partial radial pair distribution function which consid-

Downloaded 11 Oct 2004 to 145.18.129.130. Redistribution subject to AIP license or copyright, see http://jcp.aip.org/jcp/copyright.jsp

ers only particles with facing patches. $g(\sigma^+)$, $g_{pp}(\lambda\sigma^+)$, and $g_{pp}(\lambda\sigma^-)$ stand for the limiting values of the distribution functions as the discontinuities are approached from above and below, respectively.

IV. RESULTS

We have performed Gibbs ensemble simulations for interaction ranges of $\lambda=1.50$ and $\lambda=1.25$. The longer range is one of the most frequently used values in the literature on the isotropic HSSW, such that reference values are readily available. The shorter range is what Lomakin *et al.* have estimated as an upper limit for the interaction range of γ-crystallin proteins.[21] For both values the fluid–fluid critical point is known to be stable (cf. Refs. 8 and 9) for isotropic interactions ($\chi=100\%$). Concerning the layout of patches on the surface, we focus on symmetrical arrangements with 2 patches (at opposite poles of the sphere), with 4 patches (in a tetragonal arrangement), and with 6 patches (with cubic symmetry). Since we do not allow patches to overlap, there is an upper limit on the surface coverage that can be achieved for each geometry. In particular, only the $n=2$ case can attain the isotropic limit, whereas the others are subject to a maximum surface coverage of $\chi_{max}(n=4)\approx 0.8453$ and $\chi_{max}(n=6)\approx 0.8787$, respectively. For a selection of values for the surface coverage χ, we then obtain phase coexistence curves by performing a series of Gibbs simulations at several temperatures, which immediately yields the liquid–gas binodals.

Figure 2 shows the coexistence curves obtained for $\lambda=1.50$ and $n=2$, for progressively decreasing surface coverage, illustrating the general behavior for surface coverages down to 60%. With decreasing χ, the critical temperature decreases (as is to be expected, since the total strength of attraction is decreased). At the same time the critical density ρ_c shows only a weak variation; the same holds as the number of patches varies at a given surface coverage χ. In contrast, the critical density is known to increase as the range λ decreases (see, e.g., Ref. 21). Apparently, for the surface coverages considered, ρ_c is not very sensitive to the degree of directionality of the attractions.

Figure 3 examines the effect of the directionality on the width of the coexistence curves. To facilitate the comparison, we use reduced temperatures ($T^*=T/T_c$). The data for $\lambda=1.50$ clearly collapse onto a single master curve, implying that a possible widening of the coexistence curves with increasing anisotropy must be weak. This is confirmed, by examining the parameter $b=B\cdot T_c^{0.32}$ (indicated in Table I), which characterizes the width of the coexistence curve [as obtained by the fit parameter B in Eq. 9)] in terms of the nondimensional temperature $t=|T/T_c-1|$: no significant increase is observed, to the precision available, until the surface coverage is lowered to $\chi=60\%$. The data for the shorter range $\lambda=1.25$, however, show that significant widening does occur for shorter ranges. Indeed, this trend is in agreement with experiments on the phase behavior of several types of γ-crystallin,[21] which indicate that models that assume isotropic short-ranged attraction seriously underestimate the width of fluid–fluid coexistence curves. Using the analytical expression for the virial coefficient [cf. Eq. (8)], one can relate critical temperatures for the different sets of parameters to a critical stickiness parameter, $1/\tau_{crit}$. Doing so for the present Gibbs-ensemble simulation data, we find that the values of τ that correspond to the critical temperature are lower than the ''universal'' value that is found for isotropic potentials. However, our Gibbs-ensemble simulation results are limited to models with only modest anisometry. We should expect the effect to be even more pronounced as χ is decreased below 60%, but for this range of χ values we cannot use the Gibbs-ensemble method. This is due to the fact that the critical temperature decreases as χ and/or λ are reduced. Consequently, simulations at low temperatures are required in order to determine the fluid–fluid coexistence curves. But for such low temperatures it becomes increasingly difficult to break bonds once they are formed. If only standard Monte Carlo moves are used, simulations at low temperatures become prohibitively expensive because the attractive particles tend to form long-lived clusters. Although these clusters will eventually break up in a sequence of energetically unfavorable bond-breaking moves, it takes a long time to equilibrate such systems. Indeed, a system of such anisometric spheres is likely to form an ''attractive glass'' more easily than a system of spherically symmetric particles with short-ranged attraction.[33–37] This tendency to form percolating clusters may explain why no direct simulations of fluid–fluid coexistence have been reported, even for spherically symmetric square-well systems for $\lambda\leqslant 1.25$. In fact, the problem of equilibration in this regime is explicitly mentioned by Vega

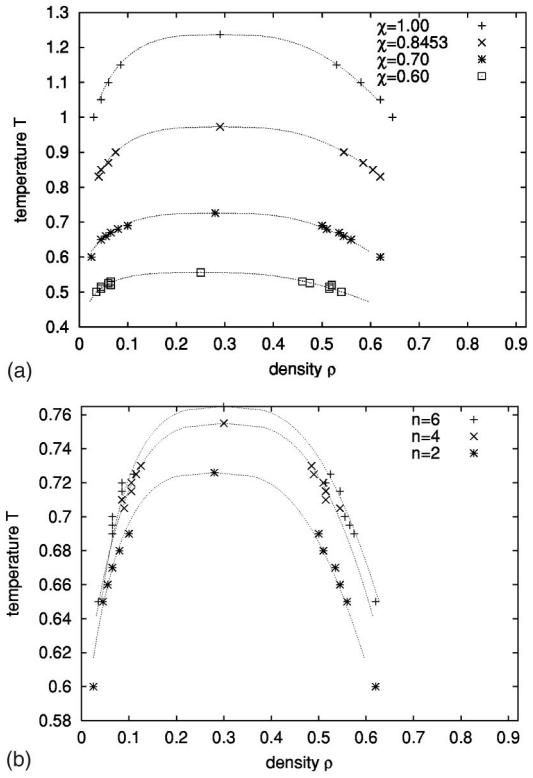

FIG. 2. Examples of coexistence curves obtained by Gibbs ensemble simulations: (a) range $\lambda=1.50$, $n=2$ patches, for various surface coverages χ, (b) range $\lambda=1.50$, surface coverage $\chi=0.70$, for $n=2,4,6$ patches. The dashed lines are binodals obtained by fitting to the law of rectilinear diameter, the critical points shown are as determined from these fits.

Downloaded 11 Oct 2004 to 145.18.129.130. Redistribution subject to AIP license or copyright, see http://jcp.aip.org/jcp/copyright.jsp

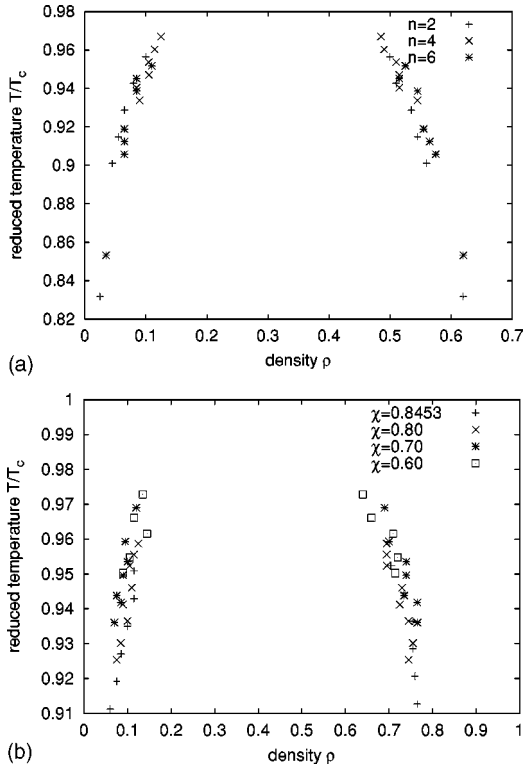

FIG. 3. Coexistence curves in terms of the reduced temperature $T^* = T/T_c$, for (a) $\lambda = 1.25$, $\chi = 0.70$, with $n = 2,4,6$ and (b) $\lambda = 1.50$, $n = 4$, with various surface coverages χ. No significant widening of coexistence curves is observed.

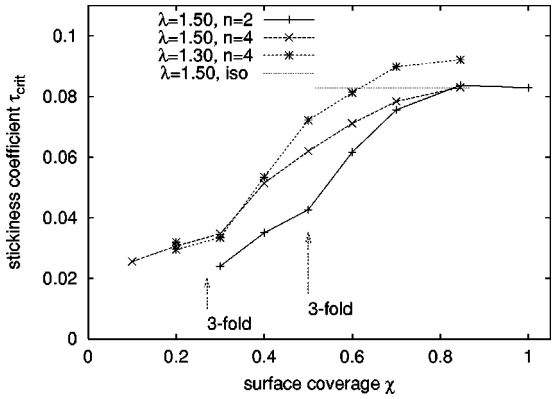

FIG. 4. The "stickiness parameter" τ_{crit} at the critical point [equivalent to the critical virial coefficient, cf. Eq. (7)], as obtained from parallel tempering simulations. The curves shown are for $\lambda = 1.50$ ($n = 2$ and $n = 4$) and for $\lambda = 1.30$ ($n = 4$). For comparison, the dotted line indicates a literature value obtained for the *isotropic* system (Ref. 24), corresponding to a range of $\lambda = 1.50$. The lines joining the data points are a guide to the eye only. The arrows labeled "3-fold" indicate the surface coverages at which either of two types of triple bonds become possible (cf. Fig. 5, and see the main text for an interpretation).

and Monson.[18] For square-well systems with attractions of shorter ranges, Lomakin *et al.*[21] have estimated the location of the fluid–fluid coexistence curve based on an extrapolation of simulation data that were collected above T_c, where gelation is not yet a problem.

We have chosen to address the problem by improving the sampling, using the parallel tempering technique described earlier. This allowed us to extend our study to much lower surface coverages. The essential results are summarized in Fig. 4, which shows the value of the virial coefficient at the critical point (as characterized by the stickiness coefficient τ) as a function of the surface coverage χ. Note, first of all, that the data series for the 2-patch systems ($n = 2$) recovers the isotropic case in the limit of complete surface coverage ($\chi = 100\%$). The limiting value for the critical virial coefficient ($\tau_c \approx 0.1$) is consistent with literature data on the critical temperature.[24]

An important result is evident from Fig. 4: the fluid–fluid critical point in systems with directional attractions is *not* characterized by a unique value for the virial coefficient. This is consistent with theoretical predictions by Kulkarni

TABLE I. Synthesis of results with detailed information on the Gibbs ensemble simulations. The symbols represent the following. n: number of patches, λ: range of attractive well, χ: surface coverage, T_c: extrapolated critical temperature, ρ_c: extrapolated critical density, A, B: fit parameters to the law of rectilinear diameter. Also provided is the parameter $b = B \cdot Tc^{0.32}$ describing the width of the binodals (in terms of the dimensionless temperature relative to the critical point, $t = |T/T_c - 1|$). More details on the simulation conditions are given in the text.

λ	n	χ	ρ_c	A	T_c	B	b
1.50	2	1.00	0.29(1)	0.20(3)	1.237(5)	0.98(1)	1.05(1)
		0.8453	0.29(1)	0.28(4)	0.973(5)	1.09(2)	1.07(2)
		0.70	0.28(1)	0.28(6)	0.726(2)	1.16(2)	1.05(2)
		0.60	0.25(2)	0.7(4)	0.556(4)	1.27(4)	1.05(3)
	4	0.8453	0.31(1)	0.2(1)	0.958(2)	1.16(1)	1.14(1)
		0.80	0.32(1)	0.0(2)	0.898(3)	1.14(1)	1.10(1)
		0.70	0.30(1)	0.2(3)	0.755(3)	1.17(3)	1.06(3)
		0.60	0.30(2)	0.4(4)	0.606(3)	1.38(3)	1.18(3)
	6	0.70	0.30(1)	0.3(1)	0.765(3)	1.17(2)	1.07(2)
		0.60	0.28(2)	0.4(4)	0.621(4)	1.28(3)	1.10(3)
1.25	2	0.70	0.39(1)	0.1(6)	0.497(1)	1.98(4)	1.58(3)
	4	0.8453	0.42(2)	−0.1(4)	0.634(3)	1.76(4)	1.52(4)
		0.80	0.39(2)	0.5(4)	0.633(2)	1.77(3)	1.53(3)
		0.70	0.38(2)	1.0(6)	0.520(2)	2.00(4)	1.62(3)
		0.60	0.37(3)	2. (2)	0.440(1)	2.19(5)	1.68(4)
	6	0.70	0.34(1)	1.9(2)	0.517(1)	1.86(3)	1.51(2)

Downloaded 11 Oct 2004 to 145.18.129.130. Redistribution subject to AIP license or copyright, see http://jcp.aip.org/jcp/copyright.jsp

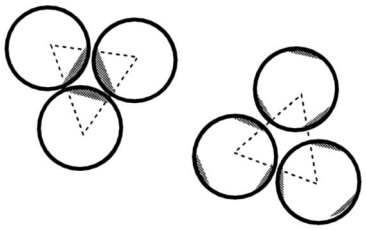

FIG. 5. Illustration of both multiple bonding scenarios: (i) threefold bonds (type ''3'') between three patches, each binding to both other patches, (ii) threefold bonds (type ''$\bar{3}$'') simultaneously involving two patches on each particle.

TABLE II. Opening angles δ and corresponding surface coverages below which three particle bonds (of type ''3'' and ''$\bar{3}$'') are no longer possible. See Fig. 5 for an illustration. All values refer to symmetric arrangements of patches. Note that the ''type 3'' multiple bonds will *never* occur if more than 6 patches are present, since each patch must then have a (half) opening angle smaller than 30°.

	δ_3	$\bar{\delta}_3$	χ_3	$\bar{\chi}_3$
$n=2$	30°	60°	0.13	0.50
$n=4$	30°	27.74°	0.27	0.18
$n=6$	30°	15°	0.40	0.03

and Zukoski.[12] Note that this observation is of direct relevance for experimental protocols to achieve optimal crystallization conditions: assuming isotropic attractions, experimental conditions close to the fluid–fluid critical point can be targeted simply by monitoring the virial coefficient (e.g., through light scattering measurements), adjusting the solvent conditions in order to approach the, supposedly, universal critical value $\tau_c \approx 0.1$. Clearly, this is no longer justified once the directional character of the attraction is important. Deviations from the isotropic value are slight for quasi-isotropic attractions ($\chi \geqslant 70\%$), but they become considerable as the surface coverage is reduced.

The data show furthermore that directionality *lowers* the critical virial coefficient, implying a lower (i.e., more negative) virial coefficient at the critical point. It is interesting to compare the 4-patch geometry with its 2-patch equivalent for the same values of λ and χ. As Fig. 4 shows, the data for $n=2$ lie consistently below those for $n=4$. The intuitive interpretation of Fig. 4 is that a stronger attraction is required in order to compensate for the loss in orientational entropy.

Another interesting feature appears when all three curves in Fig. 4 are compared as the surface coverage χ decreases. For χ close to complete coverage, the critical value of τ at fixed λ hardly depends on the number of patches. However, around $\chi \approx 70\%$, the behavior of different geometries ($n=2$ and $n=4$ for $\lambda=1.50$) starts to differ. Finally, in the limit of low surface coverage ($\chi \leqslant 0.30$), all influence of the range appears to have vanished, as the curve for $n=4$ and $\lambda=1.50$ practically coincides with the one for $n=4$ and $\lambda=1.30$. However, these asymptotic curves clearly differ from the one with $n=2$ patches. Apparently, the critical temperature of very strongly directional attractions is governed by the arrangement of patches rather than by the interaction range. This is important, as it implies that, even in the limit of very short attraction ranges, knowledge of the attractive fraction of the surface alone is *not* sufficient to predict the phase behavior.

As can be seen in Fig. 4, τ_c initially increases slowly with increasing χ. However, beyond a well-defined χ value, there is a sudden increase in the slope. We argue that this change in slope is related to the onset of multiparticle bonding events. It is clear that a triplet, such as shown in Fig. 5 has a decreased possibility to form an attractive bond with another particle because of steric screening. We should expect the critical point to drop rapidly as more of the attraction becomes ''screened'' by such triplet formation. However, depending on the precise patch-distribution, there is a critical value of χ below which triplets cannot form. Below that value of χ, the effective attraction between patchy spheres is much less screened. We can make this argument more quantitative by considering when triplets can form. A first type of 3-particle bonding involves one patch on each particle, each one binding to *both* other particles (cf. Fig. 5). This clearly requires a (half) opening angle of $\delta=30^o$, independent of the arrangement of patches on the particle surface. Another type of 3-particle cluster can occur, involving *two* patches on each particle (cf. Fig. 5). In this case, the precise geometry matters for the required opening angle, which needs to be determined by geometrical considerations. Table II lists the required opening angles for all geometries studied, as well as their corresponding surface coverages χ_3 and $\bar{\chi}_3$. For a given patch geometry, χ_3 and $\bar{\chi}_3$ indicate where each type of 3-particle bonding becomes impossible as the surface coverage is reduced. The corresponding values for χ are indicated in Fig. 4. As can be seen from Fig. 4, the change in slope of the $\tau_c - \chi$ curve does indeed coincide with the point where triplet formation first occurs.

V. CONCLUSIONS

We have used Monte Carlo simulations to establish how directionality in the particle attractions affects the fluid–fluid coexistence. The model used is a modified attractive hard sphere square well potential, which restricts attraction to orientations with two facing patches. Directionality is strong in those systems with few and/or narrow patches. The fluid–fluid critical temperature is lowered as the patches become smaller, whereas the number of patches has a much smaller effect. Variations in the associated critical density are small down to surface coverages of 60%.

In terms of the reduced temperature T/T_c, no significant widening of the binodals occurs down to a surface coverage of 60%. Most importantly, the virial coefficient associated with the critical temperature drops with increasing directionality: in contrast to the isotropic case, the fluid–fluid critical point is *not* characterized by a universal value of the reduced second virial coefficient.

ACKNOWLEDGMENTS

This work was supported in part by ''Chemische Wetenschappen-Unilever'' program with financial aid from both NWO (''Nederlandse Organisatie voor Wetenschappelijk Onderzoek'') and Unilever Research. The work of the

Downloaded 11 Oct 2004 to 145.18.129.130. Redistribution subject to AIP license or copyright, see http://jcp.aip.org/jcp/copyright.jsp

FOM Institute is part of the research program of FOM and is made possible by financial support from the Netherlands organization for Scientific Research (NWO). An NCF grant for supercomputer time is gratefully acknowledged. We would like to thank J. Horbach, M. Miller, M. Noro, and S. Pronk for useful discussions.

[1] J.P. Hansen and I.R. MacDonald, *Theory of Simple Liquids* (Academic, New York, 1976).
[2] M. Muschol and F. Rosenberger, J. Chem. Phys. **107**, 1953 (1997).
[3] A. George and W.W. Wilson, Acta Crystallogr., Sect. D: Biol. Crystallogr. **50**, 361 (1994).
[4] D. Rosenbaum, P.C. Zamora, and C.F. Zukoski, Phys. Rev. Lett. **76**, 150 (1996).
[5] A.P. Gast, C.K. Hall, and W.B. Russel, J. Colloid Interface Sci. **96**, 251 (1983).
[6] S.M. Illet, A. Orrock, W.C.K. Poon, and P.N. Pusey, Phys. Rev. E **51**, 1344 (1995).
[7] P.-R. Ten Wolde and D. Frenkel, Science **277**, 1975 (1997).
[8] G.A. Vliegenthart and H.N.W. Lekkerkerker, J. Chem. Phys. **112**, 5364 (2000).
[9] M.G. Noro and D. Frenkel, J. Chem. Phys. **113**, 2941 (2000).
[10] A. Lomakin, N. Asherie, and G.B. Benedek, Proc. Natl. Acad. Sci. U.S.A. **96**, 9465 (1999).
[11] C. Haas, J. Drenth, and W.W. Wilson, J. Phys. Chem. B **103**, 2808 (1999).
[12] A. M. Kulkarni and C. F. Zukoski, preprint.
[13] R.A. Curtis, H.W. Blanch, and J.M. Prausnitz, J. Phys. Chem. B **105**, 2445 (2001).
[14] R.P. Sear, J. Chem. Phys. **111**, 4800 (1999).
[15] M.S. Wertheim, J. Chem. Phys. **85**, 2929 (1986).
[16] G. Jackson, W.G. Chapman, and K.E. Gubbins, Mol. Phys. **65**, 1057 (1988).
[17] W. G. Chapman, J. Chem. Phys. **93**, 4299 (1990).
[18] C. Vega and P.A. Monson, J. Chem. Phys. **109**, 9938 (1998).
[19] D. Ghonasgi and W.G. Chapman, Mol. Phys. **79**, 291 (1993).
[20] R.J. Baxter, J. Chem. Phys. **49**, 2770 (1968).
[21] A. Lomakin, N. Asherie, and G.B. Benedek, J. Chem. Phys. **104**, 1646 (1996).
[22] N.V. Brilliantov and J.P. Valleau, J. Chem. Phys. **108**, 1115 (1998).
[23] J.R. Elliott and L. Hu, J. Chem. Phys. **110**, 3043 (1999).
[24] L. Vega, E. de Miguel, L.R. Rull, G. Jackson, and A.A. McLure, J. Chem. Phys. **96**, 2296 (1992).
[25] A.Z. Panagiotopoulos, Mol. Phys. **61**, 813 (1987).
[26] A.Z. Panagiotopoulos, N. Quirke, M. Stapleton, and D. Tildesley, Mol. Phys. **63**, 527 (1988).
[27] B. Smit, Ph. de Smedt, and D. Frenkel, Mol. Phys. **68**, 931 (1989).
[28] D. Frenkel and B. Smit, *Understanding Molecular Simulation. From Algorithms to Applications* (Academic, Boston, 1996).
[29] E. A. Guggenheim, J. Chem. Phys. **13**, 253 (1945).
[30] C.J. Geyer and A.A. Thomson, J. Am. Stat. Assoc. **90**, 909 (1995).
[31] W.R. Smith, D. Henderson, and Y. Tago, J. Chem. Phys. **67**, 5308 (1977).
[32] A. Lang, G. Kahl, C.N. Likos, H. Löwen, and M. Watzlawek, J. Phys.: Condens. Matter **11**, 10143 (1999).
[33] J. Bergenholtz and M. Fuchs, Phys. Rev. E **59**, 5706 (1999).
[34] W. Kob, in *Soft and Fragile Matter, Nonequilibrium Dynamics, Metastability and Flow,* edited by M. E. Cates and M. R. Evans (IOP, London, 2000), p. 25.
[35] K. Dawson, G. Foffi, M. Fuchs, W. Götze, F. Sciortino, M. Sperl, P. Tartaglia, T. Voigtmann, and E. Zaccarelli, Phys. Rev. E **63**, 011401 (2000).
[36] A.M. Puertas, M. Fuchs, and M.E. Cates, Phys. Rev. Lett. **88**, 098301 (2002).
[37] K.N. Pham, A.M. Puertas, J. Bergenholtz, S.U. Egelhaaf, A. Moussaid, P.N. Pusey, A.B. Schofield, M.E. Cates, M. Fuchs, and W.C.K. Poon, Science **296**, 104 (2002).

Downloaded 11 Oct 2004 to 145.18.129.130. Redistribution subject to AIP license or copyright, see http://jcp.aip.org/jcp/copyright.jsp